ARTICLE

Received 00th January 20xx,

Accepted 00th January 20xx

DOI: 10.1039/x0xx00000x

Nanoengineering multifunctional hybrid interfaces using adhesive glycogen nanoparticles

Pietro Pacchin Tomanin[a], Jiajing Zhou[a], Alessia Amodio[a], Rita Cimino[a], Agata Glab[a], Francesca Cavalieri[b,c,*], Frank Caruso[a,*]

Multifunctional and biodegradable nanostructured hybrid interfaces based on biopolymers are potentially useful in many applications in catalysis, bioanalytical sensing and nanomedicine. Herein, we report the engineering of multifunctional hybrid films by assembling adhesive biological nanoparticles i.e. lipoate-conjugated phytoglycogen (L-PG). These nano building blocks possess adhesive properties, arising from their amphiphilic nature, and reactive functional disulfide groups. The assembly of L-PG on surfaces enabled the rapid and conformal deposition of a thin film on substrates of varying chemical composition and wettability. The L-PG films showed negligible cytotoxicity and moderate stability under different harsh conditions but displayed enzyme-mediated degradability. In addition, metal nanoparticles were embedded into the L-PG layers to build up multilayered hybrid films. Specifically, Au and Ag nanoparticle-loaded L-PG multilayered films with catalytic and surface-enhanced Raman scattering properties were prepared. Finally, we highlight the versatility of the present approach to engineer multifaceted interfaces for catalysis and sensing applications.

Introduction

The engineering of multifunctional nanostructured interfaces has attracted great interest in many interdisciplinary fields including nanomedicine,[1] biosensing,[2] tissue engineering,[3] and catalysis.[4] The desired multifunctional interface can be achieved by controlling the chemical functionality and structural arrangement of the building blocks on a nanometer scale. For integration of functions, a polymeric material with the desired functionality and morphology can be combined with inorganic or metal nanoparticles to engineer a complex hybrid interface with structural and compositional inhomogeneity.[5–7] The precise manipulation of the physical and chemical interactions between these hybrid building blocks allows control of the interface nanomorphology and functionality of the macroscopic materials. The use of polysaccharides, such as chitosan,[8,9] amylose,[10] cellulose,[11] hyaluronic acid,[12,13] as biodegradable polymeric components for engineering multifunctional surfaces and films, is attractive because polysaccharides are natural biomacromolecules that can be chemically or biochemically modified to impart various functional properties. In particular, glycogen is a biological polysaccharidic nanoparticle found ubiquitously across the animal and plant kingdoms, serving as a vital component of the cellular energy machinery.[14,15] Glycogen nanoparticles have a dendrimer-like structure composed of repeating units of glucose connected by linear α-(1,4) glycosidic linkages with α-(1,6) branching. They have different structural properties (e.g., nanoparticle size, molecular weight, and degree of branching) depending on the source.[16] For example, phytoglycogen (PG) is a naturally abundant form of glycogen derived from sweet corn, possessing a diameter of 80 nm and a high molecular weight of 20 MDa.[16] PG nanoparticles have a highly branched, hydrated structure[17,18] and a high colloidal stability, and chemical functionalization of the polymeric chains can be performed under mild conditions using nontoxic reagents. Importantly, the reactive hydroxyl groups on glycogen can be modified to produce functional nanoparticles that remain partially biodegradable,[19] making glycogen attractive as a building block for engineering biofunctional materials and interfaces. Recently, glycogen nanoparticles with different chemical modifications and properties have been successfully exploited for drug delivery,[20–23] targeting,[24] cellular imaging,[19,25] and smart materials.[26–29]

Amine functionalities are typically introduced on glycogen to form complexes with negatively charged nucleic acids.[19–20] Octenylsuccinate hydroxypropyl PG nanoparticles were developed to improve the solubility of hydrophobic dugs.[29] The modification of glycogen with hydrophobic allyl and propargyl moieties was

[a] ARC Centre of Excellence in Convergent Bio-Nano Science and Technology, and the Department of Chemical Engineering, The University of Melbourne, Parkville, Victoria 3010, Australia. E-mail: fcaruso@unimelb.edu.au
[b] School of Science, RMIT University, Melbourne, Victoria 3000, Australia. E-mail: francesca.cavalieri@rmit.edu.au
[b.] Dipartimento di Scienze e Tecnologie Chimiche, Università di Roma ''Tor Vergata'', via della ricerca scientifica 1, 00133, Rome, Italy. E-mail: francesca.cavalieri@rmit.edu.au
Electronic Supplementary Information (ESI) available: Synthesis of L-PG, DD-PG and AuNP, details on experimental procedures and materials characterization. See DOI: 10.1039/x0xx00000x

exploited to obtain crosslinked water-insoluble films with a fibrous or sponge-like structure. The films were used as a scaffold for growing osteoblast-like cells.[30] A stimuli-responsive hydrogel for colon-targeted drug delivery was obtained via free-radical polymerization of glycogen, modified by *N*-isopropylacrylamide moieties, with ethylene glycol dimethacrylate as a crosslinker.[31] Despite the various glycogen-based materials developed to date, the use of the adhesive properties of glycogen nanoparticles for the preparation of functional interfaces remains to be examined and exploited. The development of adhesive glycogen nanoparticles and self-assembly strategies is expected to advance this biological nanoparticle toward its use as a versatile surface coating material. We propose that the modification of PG with hydrophobic and functional moieties would endow the functionalized amphiphilic polysaccharide with unexplored adhesive properties to prepare nontoxic, biodegradable films.

In the present study, we report a rapid and robust method to form nanostructured hybrid films using lipoate-conjugated phytoglycogen (L-PG). L-PG exhibits remarkable adhesiveness to coat various substrates including organic, inorganic, and even low-surface-energy materials (e.g., polytetrafluoroethylene (PTFE)). A thin and homogenous film is rapidly formed by immersion of the substrate into an L-PG water solution. The resulting L-PG film shows negligible cytotoxicity and significant degradability, yet displays stability in various harsh environments such as strong acid. We also demonstrate that these films can be functionalized with inorganic nanoparticles (e.g., Au, Ag, and Pt nanoparticles) owing to the high affinity of disulfide bridges in the tagged lipoate to the noble metal nanoparticles. The supported Au nanoparticles (AuNPs) show catalytic activity and high stability owing to the high permeability and protection of the L-PG multilayered film. Moreover, a surface-enhanced Raman scattering (SERS) active substrate is developed by integrating Ag nanoparticles (AgNPs) into the coating, therefore producing sensing interfaces that can monitor chemical changes in the surface proximity. Overall, this study describes a rapid and facile strategy for preparing multifunctional and biodegradable interfaces for different applications including in the environmental and medical fields.

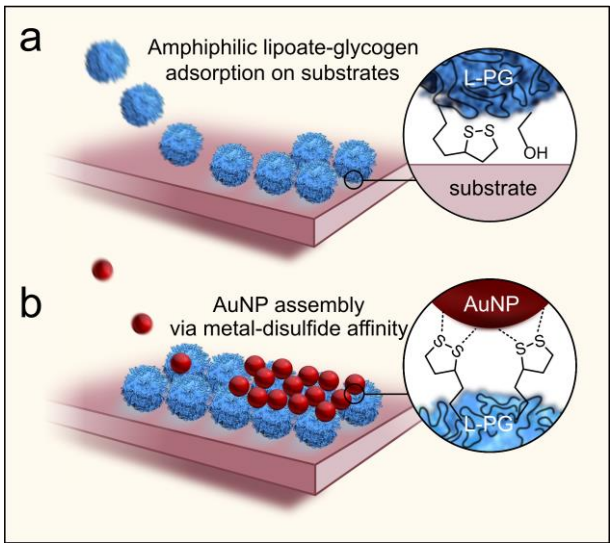

Fig. 1. (a) Schematic of the L-PG assembly on a substrate and (b) co-assembly of metal nanoparticles on the L-PG layer to obtain hybrid surfaces via LbL assembly suitable for catalysis and sensing applications.

Experimental

Materials

Phytoglycogen derived from sweet corn (PG) was purchased from Glysantis. Acetic acid glacial, anhydrous dimethyl sulfoxide (DMSO) (≥99.9%), ammonium molybdate, β-amylase from barley, copper(II) sulfate pentahydrate, crystal violet (CV), deuterium oxide, dialysis tubing cellulose membrane (14 kDa cutoff), fetal bovine serum, glutathione (GSH), gold(III) chloride hydrate, hydrochloric acid, lipoic acid (LA), methylene blue, nitric acid, Parafilm M, phosphate buffered saline (PBS) tablets, platinum nanopowder (<50 nm), polyethylene terephthalate (PET) film, polymethylmethacrylate (PMMA) film, polypropylene (PP) film, polystyrene (PS) film, PTFE film, AgNPs (20 nm), sodium acetate, sodium arsenate dibasic pentahydrate, sodium bicarbonate, sodium borohydride, sodium carbonate, sodium citrate, sodium dodecyl sulfate (SDS), sodium potassium tartrate tetrahydrate, sodium sulfate, sulfuric acid, thiazolyl blue tetrazolium bromide (MTT), and *N*-(3-dimethylaminopropyl)-*N*′-ethylcarbodiimide hydrochloride (EDC-HCl) were purchased from Sigma-Aldrich. Cover glass slips were purchased from Knittel Glass. PMMA slides were purchased from Caplugs Evergreen. 4-(Dimethylamino)pyridine (DMAP) was purchased from Fluka. Alexa Fluor 488 NHS Ester and Dulbecco's modified Eagle medium were purchased from Thermo Fisher Scientific. Dodecanoic acid was purchased from Alfa Aesar. Hydrogen peroxide, ethanol (EtOH), and *n*-hexane were purchased from Chem-Supply. A PS particle suspension (3.2 µm) was purchased from MicroParticles. PP conical tubes (15 mL) were purchased from Corning. Nickel foam was purchased from American Elements. PS cuvettes were purchased from Greiner Bio-One. PTFE and polyurethane tubes were purchased from ATA Scientific. All the chemicals were used as received. High-purity (Milli-Q) water with a resistivity of 18.2 MΩ cm was obtained from an inline Millipore RiOs/origin water purification system.

Synthesis of L-PG

To modify PG with a degree of functionalization of 2% (LA/glucose mol/mol), PG (200 mg, 1.23 mmol glucose unit) was dissolved in 8 mL anhydrous DMSO under an inert atmosphere of nitrogen. LA (30.6 mg, 0.12 eq.), DMAP (45.2 mg, 0.3 eq.), and EDC-HCl (28.4 mg, 0.12 eq.), each dissolved in 4 mL anhydrous DMSO, were sequentially added dropwise to the above solution under stirring. The system was allowed to react for 72 h under nitrogen gas flux. Then, HCl (1.2 M, 0.31 mL, 0.3 eq.) was slowly added to neutralize DMAP. The product was purified by dialysis (14 kDa cutoff) against acidic Milli-Q water (2 L, pH 4 using HCl) for 2 days and neutral Milli-Q water for one day, and freeze-dried to finally obtain L-PG (yield 180 mg, 90%). The degree of functionalization of modified glycogen was determined by NMR spectroscopy. ^{1}H-NMR (400 MHz, D_2O, 50 °C) δ (ppm): 5.36 (0.98, H-aα), 4.97 (0.02, H-aβ), 4.30–3.32 (6.53, H-b, c, d, e, f), 3.31–3.20 (0.02, H-k, m), 2.62–2.4 (0.07, H-g), 2.08–

1.94 (0.03, H-l), 1.87–1.19 (0.13, H-h, i, j). The degree of functionalization was calculated by dividing the peaks integral relative to the lipoate peaks (δ (ppm): 3.31–1.19) by the peaks integral of H-aα and H-aβ (δ (ppm): 5.60–4.80) to 100.

Preparation of L-PG metal nanoparticle hybrid coatings on glass

Circular glass substrates (diameter of 10 mm) were functionalized with L-PG and Au, Ag and Pt metal nanoparticles. First, the substrates were cleaned with EtOH and water and placed on a planar surface. To prepare the first layer, an L-PG dispersion (0.4 mL, 0.1 mg mL^{-1}) was deposited on the glass. After incubation for 10 min, the glass was rinsed with water. To prepare the second layer of metal nanoparticles, 0.4 mL of a Au (0.06 mg mL^{-1}), Ag (0.02 mg mL^{-1}), or Pt (0.1 mg mL^{-1}) colloidal dispersion was added and the system was incubated for another 10 min. The glass was then washed with water to obtain one bilayer on one side of the substrate. To prepare multilayered or multi-elements systems, the process was repeated as many times as required with the appropriate metal nanoparticles. When the appropriate number of bilayers was obtained, the glass was dried with a N_2 gun. For control experiments, unmodified PG was used with AuNPs following the abovementioned procedure. The glass substrates were directly incubated with AuNPs in the absence of L-PG following the same procedure.

Preparation of PS microparticles coated with L-PG and AuNPs

A dispersion of 3.2 µm PS particles (0.3 mL, 1 mg mL^{-1}) was washed via centrifugation and redispersion with water three times (2000 rcf, 2 min). After each centrifugation, sonication in an ultrasound bath was performed for 5 s to disperse the particles in solution. During the last wash, the dispersion was diluted with water to 0.3 mL and added via pipetting to an L-PG solution (0.2 mL, 0.1 mg mL^{-1}). After gentle mixing for 3 min, a further three washes as previously described were performed. In the last wash, the dispersion was diluted to 0.3 mL to obtain a 1 mg mL^{-1} L-PG-coated PS microparticle dispersion. To this dispersion, 0.5 mL of AuNP colloidal suspension was added by pipetting and the solution was gently mixed for 3 min. The colloidal dispersion was then washed three times as previously described and finally diluted to 0.3 mL to obtain a 1 mg mL^{-1} PS microparticles coated with one L-PG/AuNP bilayer. The assembly cycle was repeated as many times as required, with the last layer composed of AuNP after each cycle.

Preparation of inner-coated PP tubes with L-PG and AuNPs

To prepare an inner-coated 15 mL PP tube via layer-by-layer (LbL) assembly, an L-PG solution (2 mL, 0.1 mg mL^{-1}) was introduced into the PP tube and vortexed for 3 min, followed by washing with water. Then, a AuNP colloidal suspension (2 mL, 0.06 mg mL^{-1}) was introduced into the tube, vortexed for 3 min, and washed with water, producing a 1-bilayer inner-coated PP tube. To obtain systems with more bilayers, the steps were repeated several times as required. The obtained functionalized vials were used fresh for the catalysis experiments.

Characterization

Attenuated total reflectance Fourier transform infrared (ATR-FTIR) spectra were obtained on a TENSOR II (Bruker) ATR–FTIR spectrometer. UV–vis absorbance spectra were recorded on a SPECORD 250 PLUS (Analytik Jena, Germany) spectrophotometer or an Infinite M200 microplate reader (Tecan, Switzerland). Dynamic light scattering (DLS) hydrodynamic diameter and ζ-potential were measured using a Zetasizer Nano-ZS instrument (Malvern Instruments, Malvern, UK). Atomic force microscopy (AFM) experiments were performed on a JPK NanoWizard II BioAFM instrument. Contact angle experiments were performed on an optical contact angle tensiometer (DataPhysics) using the sessile drop method. Cell viability was evaluated via a standard MTT assay protocol using MDA-MB-231 cells. The rate of glycogen particle degradation by β-amylase was determined using the Somogyi–Nelson assay. The chemical stability of the L-PG coatings was studied via fluorescence analysis using a Fluorolog spectrofluorometer (Jobin Yvon Horiba). Quartz crystal microbalance with dissipation (QCM-D) experiments were performed using a QSense E4 (Biolin Scientific, Sweden) equipped with gold sensor chips (QSX 301 Gold, Biolin Scientific). Differential interference contrast (DIC) microscopy images were recorded using an inverted Olympus IX71 microscope. TEM images were acquired using a Tecnai Spirit (FEI, USA) instrument with an operation voltage of 120 kV. SEM images and EDX spectra and mapping were acquired with a FlexSEM 1000 (Hitachi, Japan) benchtop scanning electron microscope equipped with a Quantax 80 (Bruker, USA) EDX system. Helium ion microscopy images were recorded on an ORION NanoFab (Zeiss, Peabody, USA) using a 25 keV He^+ probe with a current of 0.3 pA. SERS analysis was conducted on a RENISHAW Raman microscope equipped with a He–Ne laser operating at 532 nm.

Results and Discussion

Synthesis and characterization of L-PG

PG was first functionalized with a natural compound, LA, via an esterification reaction in DMSO to form L-PG (Figure S1). The resulting L-PG bears both hydrophilic and hydrophobic moieties (Figure 1a) that impart adhesion properties to the nanoparticles. In addition, the disulfide groups of lipoate are reactive toward metal nanoparticles (Figure 1b). NMR spectra confirmed the successful preparation of L-PG, which showed distinct signals that were ascribed to the glucose repeating unit and lipoate moieties (Figure S2). The lipoate groups are likely grafted to the outermost branches of PG. Previous work has shown that glycogen inner chains that are not swollen by organic solvent (e.g., DMF and DMSO) are less accessible and reactive, leading to surface-constrained functionalization.[32] It is noteworthy that a trade-off between hydrophilicity and hydrophobicity is vital in the design of this building block. For example, samples with a degree of functionalization higher than 2% showed poor solubility in water and DMSO owing to the high hydrophobicity (Table S1).

ARTICLE

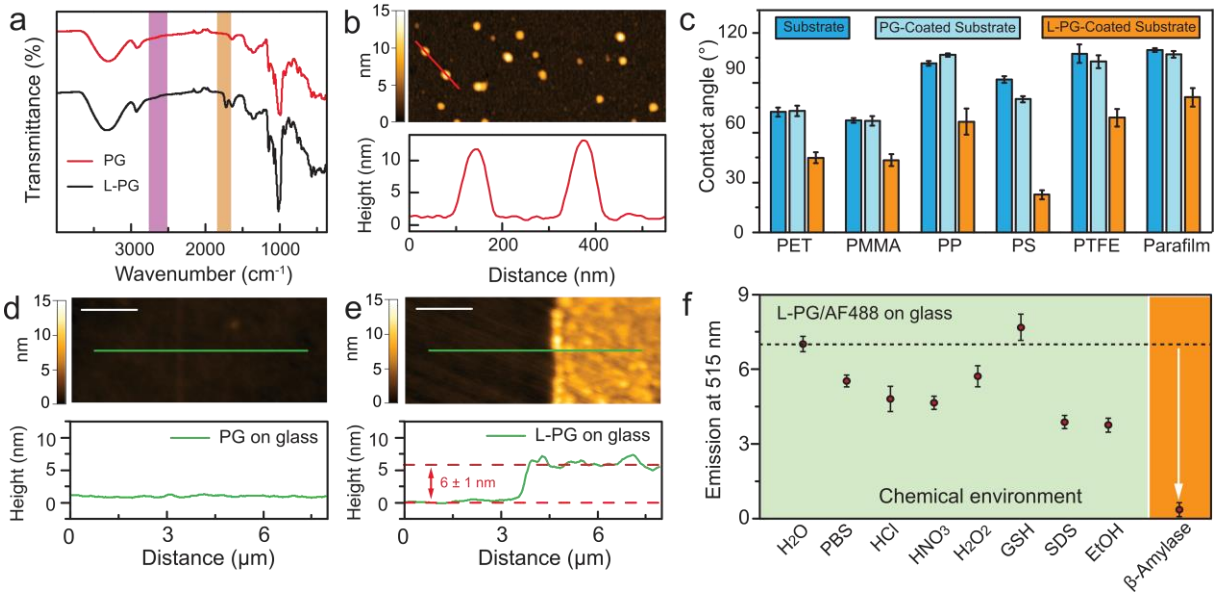

Fig. 2. Characterization and coating properties of L-PG. (a) ATR-FTIR spectra of PG and L-PG and (b) dry-state AFM image and corresponding height profile of L-PG. (c) Water contact angles of the bare, PG-, and L-PG-coated substrates. Dry-state AFM images and corresponding height profiles of (d) PG- and (e) L-PG-coated glass substrates (scale bar 2 μm). (f) Emission intensities of fluorescently labeled L-PG coatings on glass substrates after incubation in different chemical and biochemical environments. Error bars represent standard deviations.

Therefore, a degree of functionalization of 2% was considered optimal for maintaining L-PG colloidal stability in aqueous solution. The presence of lipoate groups on L-PG was further confirmed by FTIR spectroscopy. The newly formed ester bonds were observed at 1721 cm^{-1} (Figure 2a). Importantly, the 1,2-dithiolane of lipoate remained in the oxidized state during the reaction, as signals corresponding to thiol stretching bands at 2560–2570 cm^{-1} were absent.[33] The new absorbance peak observed at 290 nm in the UV–vis spectrum of L-PG further confirmed the presence of the lipoate ring (Figure S3).[34] The synthesized L-PG had a hydrodynamic diameter (90 ± 50 nm), as determined by DLS, and a ζ-potential value (−1 ± 6 mV) similar to those of unmodified PG (90 ± 40 nm; −1 ± 6 mV) (Figure S4). These results confirm that the chemical modification of PG with up to 2% hydrophobic moieties does not induce any aggregation or substantial change in the solution properties of the resulting nanoparticles relative to those of the unmodified PG. Dry-state AFM further confirmed that the L-PG nanoparticles were spherical and well dispersed, with a round flattened shape, characteristic of dehydrated spherical soft materials (Figure 2b). As measured by AFM, the L-PG nanoparticles featured an average diameter of 90 ± 20 nm and a thickness of 8 ± 2 nm.

Preparation and characterization of L-PG coatings

L-PG was subsequently examined for coating several planar polymeric substrates, including PET, PMMA, PP, PS, Parafilm, and PTFE. The successful coating was confirmed by contact angle measurements (Figure 2c). Specifically, the L-PG film formed on a PTFE surface featured a reduced water contact angle from 107 ± 6° (uncoated PTFE substrate) to 69 ± 5°, thus shifting the wettability of the final film from hydrophobic to hydrophilic. A similar trend was observed on other substrates (Figures 2c and S5). Conversely, when unmodified PG was used to coat these substrates, there was negligible difference in the contact angle before and after the deposition procedure (Figure 2c). This observation indicates that the unmodified PG nanoparticles show poor adhesiveness. In addition, AFM analysis revealed that, unlike unmodified PG (Figure 2d), a continuous, dense L-PG film of 6 ± 1 nm in thickness formed on the glass surface after deposition (Figure 2e).

To examine the stability of the films, L-PG was labeled with a fluorophore tag (AF488) so that the disassembly of the coating was monitored after the treatment. The L-PG coating was first incubated in different solutions for 60 min, followed by repeated washing with water. The fluorescence intensity of the substrates was then recorded to evaluate residual L-PG on the substrates. The results indicate that the L-PG coating shows moderate stability in diverse

chemical environments such as in H_2O, 10 mM PBS (pH 7.4), 1 M HCl, 1 M HNO_3, 1 M H_2O_2, 10 mM GSH, 17 mM SDS, and EtOH (Figure 2f). In contrast, the L-PG film can be significantly degraded by β-amylase (Figure 2f) and the building block are not cytotoxic (Figure S6). However, the L-PG nanoparticles required a longer incubation time than the unmodified PG nanoparticles to achieve the same degree of degradation by β-amylase (Figure S7). These results show that stable aqueous suspensions of hydrophobically modified PG nanoparticles can be used to build robust but biodegradable, noncytotoxic thin films owing to the adhesiveness of L-PG that promotes the interfacial assembly of nanoparticles on substrates with different wettability.

To understand the mechanism governing the adhesion properties of L-PG, the influence of the amphiphilic nature of PG without disulfide bonds was assessed. To this end, an analogous amphiphilic PG derivative, containing 1% hydrophobic dodecane moiety (DD-PG) was synthesized (Figure S8). DD-PG displayed properties similar to those of L-PG such as hydrodynamic diameter (71 ± 40 nm) and ζ-potential (−1 ± 5 mV). The results showed that the water-soluble DD-PG also formed a film on glass similar to L-PG, with a similar thickness and surface morphology (Figure S9). These findings underline the importance of the amphiphilic characteristic of modified PG for the successful formation of coatings. Moreover, the disulfide moieties in L-PG offer an additional advantage for further functionalization of the L-PG films.

Characterization of L-PG/metal nanoparticles hybrid films

Herein, we demonstrate that glycogen–inorganic hybrid films with controlled thickness can be fabricated by LbL assembly of L-PG and metal nanoparticles, including AuNPs, AgNPs, and platinum nanoparticles (PtNPs) (Figure 3a). The assembly of the L-PG/AuNP film was monitored by measuring the (linear) increase in the intensity of the localized surface plasmon resonance (LSPR) band of the AuNPs at ~545 nm. (Figure S10). Notably, the narrow LSPR peak indicates the relatively large interparticle distance between neighboring AuNPs, suggesting that the AuNPs do not form clusters when embedded in the film and L-PG nanoparticles act as a spacer. Similar trends in relation to the increase in absorbance intensity were observed in the multilayered hybrid films containing AgNPs (LSPR at 415 nm) or PtNPs (a broad absorbance profile spanning the UV–vis region without a characteristic peak) (Figure S11). A multicomponent hybrid film with three bilayers obtained by sequential deposition of L-PG/AuNP, L-PG/AgNP, and L-PG/PtNP is also demonstrated. The resulting UV–vis spectrum exhibited a combined absorption profile comprising the typical absorbance of each metal nanoparticle assembly (Figure 3a, red line). To demonstrate the importance of disulfide moieties in coordinating the metal NPs for the successful assembly of the hybrid films, control experiments were performed using DD-PG/AuNP, unmodified PG/AuNP, and AuNPs. The deposition of these control systems on a glass slide resulted in very weak LSPR bands, indicating poor adsorption on the glass surface (Figure S12). These results highlight the importance of disulfide bonds on L-PG for the successful loading of AuNPs.

QCM-D was used to monitor the kinetics of the hybrid film assembly process by depositing sequential layers of L-PG and AuNPs. L-PG first directly adhered to the gold substrate acting as a primer layer, followed by the deposition of AuNPs on the L-PG layer to form a hybrid bilayer structure, stabilized by disulfide–gold interactions (Figure 3b). Both L-PG and AuNP deposition reached equilibrium within 30 min of incubation. The dissipation factor increased when an L-PG layer was deposited, indicating that the L-PG layer was distorted during crystal oscillations and therefore displayed characteristics of a soft film (Figure S13). In contrast, the dissipation factor remained constant upon deposition of AuNPs, showing that the rigid AuNPs followed the oscillation of the crystal without being deformed. These results demonstrated the hybrid nature of the coating.

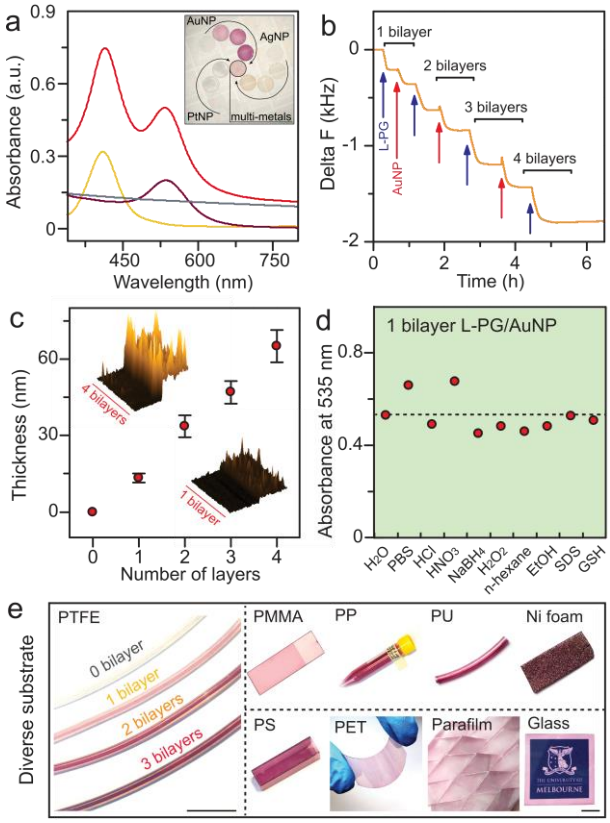

Fig. 3. Characterization of hybrid L-PG LbL assemblies with metal nanoparticles. (a) UV–Vis spectra of glass substrates coated with one bilayer of L-PG/AuNP, L-PG/AgNP and L-PG/PtNP (purple, yellow and grey lines, respectively) and three bilayers of sequentially assembled L-PG/AuNP, L-PG/AgNP, and L-PG/PtNP (red line) and corresponding photograph (inset) of glass substrates coated with various layers of L-PG and metal nanoparticles (Au, Ag, Pt, and Au–Ag–Pt). (b) QCM-D frequency profile of an L-PG/AuNP LbL assembly on a gold chip obtained by sequential deposition of L-PG (blue arrow) and AuNPs (red arrow). (c) Dry-state AFM film thickness profile as a function of the L-PG/AuNP bilayer number and corresponding AFM images of the first and fourth bilayers (insets). (d) LSPR absorbance of glass substrates with 1 bilayer of L-PG/AuNPs after incubation in various chemical environments. (e) Photographs of L-PG/AuNP LbL assemblies on various substrates (scale bar 1 cm).

ARTICLE

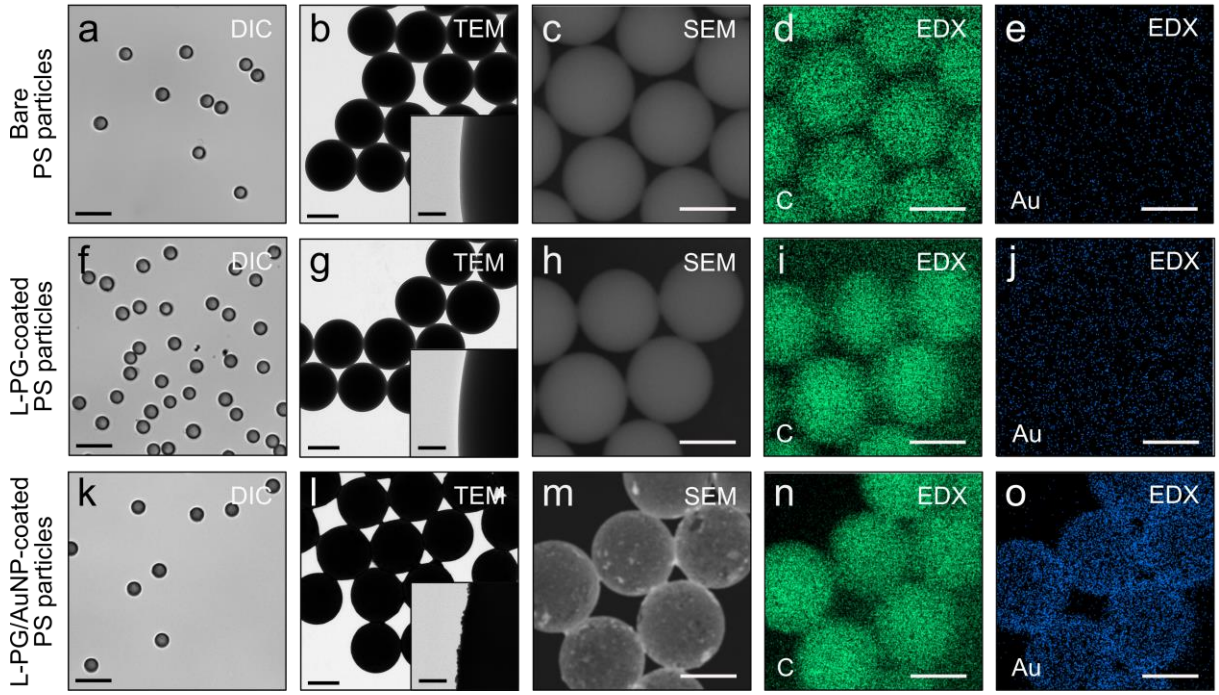

Fig. 4. PS microparticles coated with L-PG and L-PG/AuNP LbL assemblies. (a, f, k) Differential interference contrast (DIC) microscopy, (b, g, l) TEM, and (c, h, m) SEM images, and (d, i, n) C and (e, j, o) Au EDX mapping of bare PS microparticles (a–e), L-PG-coated PS microparticles (f–j), and 3-bilayer L-PG/AuNP-coated PS microparticles (k–o). Scale bars: DIC (10 µm), TEM (2 µm) and inset (100 nm), and SEM and EDX (3 µm).

The film growth was also monitored by AFM measurements of the average dry thickness and roughness of the films. After the deposition of each bilayer, the dry thickness and roughness increased by 6.3 ± 0.6 and 2.4 ± 0.1 nm, respectively, indicating that the films were compact and homogeneous with a high surface coverage (Figure 3c and Figures S14, 15). Importantly, the L-PG/AuNP hybrid coatings on glass displayed excellent chemical stability up to 60 min in several harsh chemical environments such as 10 mM PBS (pH 7.4), 1 M HCl, 1 M HNO_3, 10 mM $NaBH_4$, 1 M H_2O_2, *n*-hexane, EtOH, 17 mM SDS, and 10 mM GSH (Figure 3d). Notably, the stability of the multilayered film was significantly higher than that of the single-layer L-PG film. This can be ascribed to the shielding effect of the AuNP layer,[35] which prevents the detachment and degradation of L-PG.

Remarkably, the L-PG/AuNP hybrid film formed on various materials such as rigid (PS, PMMA, PP, polyether ether ketone) and flexible (PTFE, PET, Parafilm, Viton, polyurethane) polymeric, oxide (cover glass), and metal (Ni foam) substrates (Figure 3e and Figure S16). The deposition is indicated by the change in color of the substrates upon adsorption of AuNPs mediated by interactions with the primer L-PG layer. The coating formed on the different substrates remained stable at room temperature (25 °C) for up to 6 months in dried state. To further extend the possible use of the L-PG/AuNP hybrid film to microscale objects, PS particles (3.2 µm) were successfully coated with three bilayers of L-PG/AuNP (Figure 4). Disperse bare PS microparticles (Figure 4a) displayed, a smooth particle edge (Figure 4b and inset) and a homogeneous distribution of carbon only (Figure 4c–e). The PS microparticles coated with one layer of the L-PG film did not show any aggregation (Figure 4f). Similarly to the bare PS microparticles, the L-PG-coated PS microparticles displayed a smooth particle edge (Figure 4g and inset) and a uniform distribution of carbon only (Figure 4h–j). The PS microparticles coated with three bilayers of L-PG/AuNP LbL assemblies did not show evidence of aggregation (Figure 4k). However, TEM images showed an increased contrast and roughness in the edge of the particles, compared with those of the bare PS and L-PG-coated PS microparticles, which was attributed to the presence of the dense AuNPs (Figure 4l and inset). Furthermore, the SEM images and EDX mapping showed the homogeneous presence of both carbon and gold in the coating (Figure 4m–o). These results further confirmed the presence of AuNPs and therefore the

successful preparation of L-PG/AuNP LbL assemblies onto PS microparticles.

Catalytic and SERS properties of hybrid LbL assemblies

To demonstrate the applications of the tunable hybrid coatings, a chemical reactor was designed by coating the inner wall of PP tubes with L-PG/AuNP bilayers for catalysis. The catalytic activities of the hybrid films were evaluated through the $NaBH_4$-mediated reduction of methylene blue (MB) to leucomethylene blue (LMB) in the presence of metal catalysts. The reaction kinetics was monitored via UV–vis spectroscopy in real time, wherein changes in the absorption peak at 664 nm, corresponding to MB, were monitored as MB was converted to colorless LMB. When an MB solution containing $NaBH_4$ was incubated in an L-PG/AuNP-coated PP tube, the blue solution turned transparent over time, indicating the successful reduction reaction (Figure 5a). In contrast, the bare and L-PG-coated PP tubes showed no reduction of MB (Figure S17). Our results show that the catalytic efficacy of the system relies on the layers of the AuNPs coating, and faster reduction kinetics were obtained in reactors with a higher number of L-PG/AuNP bilayers (Figure 5b). Specifically, MB reduction in the reactors followed a second-order reaction with rate constants of 6.0 ± 0.8, 11.0 ± 0.8, and 20 ± 2 mM^{-1} min^{-1} for 1, 3, and 5 L-PG/AuNPs bilayers, respectively. This improvement was due to the increasing overall amount of AuNPs and easy access of small molecules into the L-PG matrix. Notably, the catalysts in the film showed high stability because of the negligible amount of AuNPs leached into the solution during the reaction (Figure 5c). The robust assembly of these hybrid films will allow defining functional coatings on various materials for catalytic purposes.

SERS can be used to detect vibrational fingerprints of chemicals with high sensitivity, wherein the Raman signals of targets are significantly augmented when located near plasmonic nanostructures (e.g., AgNPs) owing to the enhanced electromagnetic field arising from the excitation of LSPR bands. Thus, by integrating AgNPs into the coatings, we can generate a SERS-active surface on glass slides that can be used to monitor the concentration of chemical species in the surrounding. Using CV as a model, we found that the hybrid coating of three L-PG/AgNP bilayers displayed SERS activity toward the substrate (Figure 5d). The signal of CV at 1615 cm^{-1} increased with increasing CV concentration ranging from 500 nM to 10 μM (Figure S18). A limit of detection of 60 nM (signal-to-noise ratio of 3) was achieved. The facile preparation of the present hybrid coatings is expected to enable the design of "smart" SERS-active coatings on diverse substrates for sensing applications.

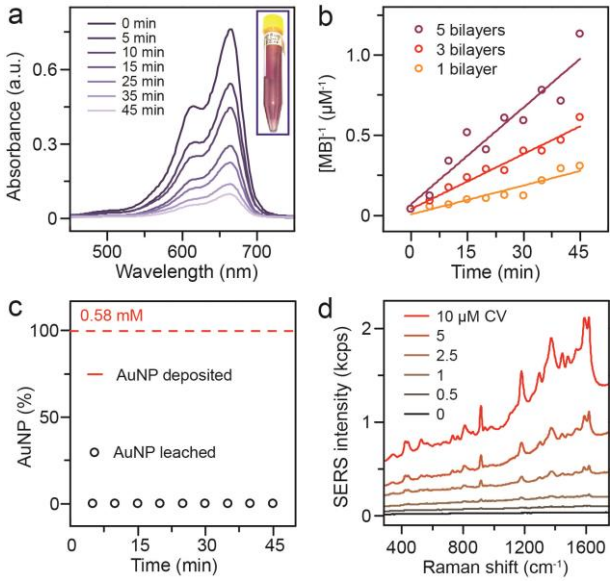

Fig. 5. Catalysis and sensing applications of L-PG/metal nanoparticles LbL assemblies. (a) UV–Vis spectra of MB recorded during its degradation via $NaBH_4$ in a 3-bilayer L-PG/AuNP-coated PP tube and photograph (inset) of the functionalized tube. (b) $NaBH_4$-mediated MB degradation kinetics in 1-, 3-, and 5-bilayer L-PG/AuNP-coated PP tubes. (c) Comparison of the amount of AuNPs leached from a 3-bilayer L-PG/AuNP-coated PP tube and the total amount of AuNPs originally deposited in the same tube. (d) SERS spectra of a 3-bilayer L-PG/AgNP-coated glass as a function of different concentrations of CV.

Conclusions

In the present work, adhesive glycogen nanoparticles were used as building blocks to prepare hybrid multifunctional films on various substrates, including organic and inorganic materials, in an aqueous environment. The adhesive and functional properties of L-PG are ascribed to the hydrophilic–hydrophobic interactions between the amphiphilic L-PG and the substrate. These polysaccharide-derived nano building blocks displayed negligible cytotoxicity, and the L-PG-based films were stable in harsh chemical environments but biodegradable. Furthermore, the presence of disulfide moieties onto L-PG allowed the integration of diverse metal nanoparticles to prepare multilayered films. As proof of concept, hybrid functional coatings were developed and applied for the catalysis and SERS-based detection of analytes. The PG-based coatings and multilayered films provide a versatile platform for engineering interfaces with modular functionalities and potential uses in nanomedicine, material science, catalysis, and sensing.

Conflicts of interest

There are no conflicts to declare.

Acknowledgements

This work was funded by an Australian Research Council (ARC) Future Fellowship (F. Cavalieri, FT140100873) and a National Health and Medical Research Council Senior Principal Research Fellowship (F. Caruso, GNT1135806) schemes. This project received funding from the European Union Horizon 2020 research and innovation program under the Marie Skłodowska-Curie grant agreement No. 690901 ("Nanosupremi") and No. 798565 (A. Amodio "RE-IMMUNE"). This work was performed at the ARC Centre of Excellence in Convergent Bio-Nano Science and Technology (project number CE140100036) and in part at the Materials Characterization and Fabrication Platform (MCFP) at The University of Melbourne.

Notes and references

(1) M. Bjornmalm, K. J. Thurecht, M. Michael, A. M. Scott and F. Caruso, *ACS Nano,* 2017, **11**, 9594.
(2) M. Holzinger, A. Le Goff and S. Cosnier, *Front. Chem.,* 2014, **2**, 63.
(3) S. Goenka, V. Sant and S. Sant, *J. Controlled Rel.,* 2014, **173**, 75.
(4) D. Lu, J. Zhou, S. Hou, Q. Xiong, Y. Chen, K. Pu, J. Ren and H. Duan, *Adv. Mater.,* 2019, **31**, 1902733.
(5) X. Wang, J. Pu, B. An, Y. Li, Y. Shang, Z. Ning, Y. Liu, F. Ba, J. Zhang and C. Zhong, *Adv. Mater.,* 2018, **30**, 1705968.
(6) R. Liu, J. Zhao, Q. Han, X. Hu, D. Wang, X. Zhang and P. Yang, *Adv. Mater.,* 2018, **30**, 1802851.
(7) P. P. Tomanin, P. V. Cherepanov, Q. A. Besford, A. J. Christofferson, A. Amodio, C. F. McConville, I. Yarovsky, F. Caruso and F. Cavalieri, *ACS Appl. Mater. Interfaces,* 2018, **10**, 42786.
(8) Z. Shi, K. Neoh, E. Kang, C. Poh and W. Wang, *J. Biomed. Mater. Res., Part A,* 2008, **86**, 865.
(9) V. K. Thakur and M. K. Thakur, *ACS Sustainable Chem. Eng.,* 2014, **2**, 2637.
(10) T. Nishimura and K. Akiyoshi, *Wiley Interdiscip. Rev.: Nanomed. Nanobiotechnol.,* 2017, **9**, e1423.
(11) C. Wang, R. A. Venditti and K. Zhang, *Appl. Microbiol. Biotechnol.,* 2015, **99**, 5791.
(12) S. E. Burke and C. J. Barrett, *Biomacromolecules,* 2003, **4**, 1773.
(13) T. I. Croll, A. J. O'Connor, G. W. Stevens and J. J. Cooper-White, *Biomacromolecules,* 2006, **7**, 1610.
(14) S. G. Ball and M. K. Morell, *Annu. Rev. Plant Biol.,* 2003, **54**, 207.
(15) P. J. Roach, A. A. Depaoli-Roach, T. D. Hurley and V. S. Tagliabracci, *Biochem. J.,* 2012, **441**, 763.
(16) Q. A. Besford, F. Cavalieri and F. Caruso, *Adv. Mater.,* 2019, 1904625, DOI: 10.1002/adma.201904625.
(17) M. Grossutti and J. R. Dutcher, *Biomacromolecules,* 2016, **17**, 1198.
(18) J. D. Nickels, J. Atkinson, E. Papp-Szabo, C. Stanley, S. O. Diallo, S. Perticaroli, B. Baylis, P. Mahon, G. Ehlers and J. Katsaras, *Biomacromolecules,* 2016, **17**, 735.
(19) M. Wojnilowicz, A. Glab, A. Bertucci, F. Caruso and F. Cavalieri, *ACS Nano,* 2018, **13**, 187.
(20) M. Wojnilowicz, Q. A. Besford, Y.-L. Wu, X. J. Loh, J. A. Braunger, A. Glab, C. Cortez-Jugo, F. Caruso and F. Cavalieri, *Biomaterials,* 2018, **176**, 34.
(21) M. Perrone, A. Lopalco, A. Lopedota, A. Cutrignelli, V. Laquintana, J. Douglas, M. Franco, E. Liberati, V. Russo and S. Tongiani, *Eur. J. Pharm. Biopharm.,* 2017, **119**, 161.
(22) R. Kandimalla, S. Dash, A. C. Bhowal, S. Kalita, N. C. Talukdar, S. Kundu and J. Kotoky, *Int. J. Nanomed.,* 2017, **12**, 7025.
(23) F. Lu, A. Mencia, L. Bi, A. Taylor, Y. Yao and H. HogenEsch, *J. Controlled Rel.,* 2015, **204**, 51.
(24) Q. A. Besford, M. Wojnilowicz, T. Suma, N. Bertleff-Zieschang, F. Caruso and F. Cavalieri, *ACS Appl. Mater. Interfaces,* 2017, **9**, 16869.
(25) S. Aasen, A. Pospisilova, T. Eichler, J. Panek, M. Hruby, P. Stepanek, E. Spriet, D. Jirak, K. Skaftnesmo and F. Thorsen, *Int. J. Mol. Sci.,* 2015, **16**, 21658.
(26) Y. Zhu, W. Tong and C. Gao, *Soft Matter,* 2011, **7**, 5805.
(27) B. Macphail and M. A. Brook, *Greem Chem.,* 2017, **19**, 4373.
(28) J. Li, D. Maniar, X. Qu, H. Liu, C.-Y. Tsao, E. Kim, W. E. Bentley, C. Liu and G. F. Payne, *Biomacromolecules,* 2019, **20**, 969.
(29) Y. Xie and Y. Yao, *Carbohydr. Polym.,* 2018, **180**, 29.
(30) M. Rabyk, M. Hruby, M. Vetrik, J. Kucka, V. Proks, M. Parizek, R. Konefal, P. Krist, D. Chvatil and L. Bacakova, *Carbohydr. Polym.,* 2016, **152**, 271.
(31) P. Patra, A. P. Rameshbabu, D. Das, S. Dhara, A. B. Panda and S. Pal, *Polym. Chem.,* 2016, **7**, 5426.
(32) M. Bertoldo, G. Zampano, L. Suffner, E. Liberati and F. Ciardelli, *Polym. Chem.,* 2013, **4**, 653.
(33) T. Liebert, M. A. Hussain, M. N. Tahir and T. Heinze, *Polym. Bull.,* 2006, **57**, 857.
(34) F. Gu, C. Hu, Z. Tai, C. Yao, J. Tian, L. Zhang, Q. Xia, C. Gong, Y. Gao and S. Gao, *Sci. Rep.,* 2016, **6**, 36281.
(35) P. Thoniyot, M. J. Tan, A. A. Karim, D. J. Young and X. J. Loh, *Adv. Sci.,* 2015, **2**, 1400010.

Supplementary Information

Nanoengineering Multifunctional Hybrid Interfaces Using Adhesive Glycogen Nanoparticles

Pietro Pacchin Tomanin, Jiajing Zhou, Alessia Amodio, Rita Cimino, Agata Glab, Frank Caruso, Francesca Cavalieri

Table of Contents

1 Experimental section

1.1 Synthesis

1.1.1 Preparation of fluorescent labeled L-PG

Lipoate-conjugated phytoglycogen (L-PG; 2 mg) was dispersed in carbonate buffer (1 mL, 10 mM, pH 9.2). To this dispersion, AF488NHS solution (30 µL, 1 mg mL^{-1} in dimethyl sulfoxide (DMSO)) was added and the resulting solution was mixed overnight. Excess fluorophore was removed using an illustra Nap 10 Sephadex column (GE Healthcare Life Sciences), and the resulting product was freeze-dried to generate L-PG@AF488.

1.1.2 Synthesis of dodecane-conjugated phytoglycogen (DD-PG)

DD-PG was prepared using the same synthesis procedure as that used for preparing L-PG, with the exception that dodecanoic acid (0.06 eq.) was used instead of lipoic acid. The degree of functionalization of modified glycogen, as determined by NMR spectroscopy, was 1% (dodecanoic moieties/glucose mol/mol).

1.1.3 Synthesis of gold nanoparticles (AuNPs)

AuNPs of 14 nm in diameter were prepared by citrate reduction of $HAuCl_4$ in aqueous phase. Typically, a sodium citrate (102 mg) water solution (2 mL) was rapidly injected into a boiling aqueous $HAuCl_4$ solution (30 mg in 200 mL water) under vigorous stirring. After boiling for 15 min, the solution was cooled to room temperature. The colloidal suspension was stored at 4 °C in the dark until further use.

1.2 Characterization

1.2.1 Attenuated total reflectance Fourier transform infrared (ATR-FTIR) spectroscopy

ATR-FTIR spectra were obtained on a TENSOR II ATR−FTIR spectrometer (Bruker) and analyzed using the software OPUS 7.8. The number of scans was 64 with a minimum resolution of 4 cm^{-1}.

1.2.2 UV–Vis spectroscopy

UV–Vis absorbance spectra were recorded on a SPECORD 250 PLUS spectrophotometer (Analytik Jena, Germany) and analyzed using the software Aspect UV. Solid and liquid samples spectra were recorded using, respectively, a solid sample holder and a reduced volume quartz cuvette with a path length of 1 cm mounted on a standard cell holder. Spectra were acquired with a scan speed of 20 nm s^{-1}. The spectra of PG and L-PG were recorded using a 1 mg mL^{-1} water dispersion.

1.2.3 Dynamic light scattering (DLS): hydrodynamic diameter and ζ-potential

The hydrodynamic diameter and ζ-potential of the nanoparticles were measured using a Zetasizer Nano-ZS instrument (Malvern Instruments, Malvern, UK) equipped with a He–Ne ion laser (λ = 633 nm). To evaluate the hydrodynamic diameter based on the scattered intensity, an L-PG or PG suspension (0.1 mL, 1 mg mL^{-1} in water) was analyzed in a micro cuvette (ZEN0040, Malvern Instruments). To evaluate the ζ-potential, a particle suspension (0.8 mL, 3 mg mL^{-1}) in PBS (0.1×, pH 7.4) was analyzed in a capillary cell (DTS1070, Malvern Instruments). The analysis was performed using a standard operation procedure with automatic attenuation and measurement position, executing 5 runs consisting of at least 10 acquisitions for each sample.

1.2.4 Atomic force microscopy (AFM)

AFM experiments were performed on a JPK NanoWizard II BioAFM instrument. Images were obtained in tapping mode using Tap300-G (BudgetSensors, Bulgaria) monolithic silicon cantilevers with a spring constant and

resonance frequency of about 40 N m^{-1} and 300 kHz, respectively. For the analysis of single particles, an L-PG aqueous dispersion (40 µL, 1 µg mL^{-1}) was incubated on a freshly gold-sputtered mica substrate (20 nm gold layer) for 60 min, extensively washed with water, and dried with a N_2 gun. Height and thickness values were averaged over 250 single nanoparticles. For the thickness and roughness analysis of the films, glass substrates were first cleaned with EtOH and water and then completely immersed in a 0.1 mg mL^{-1} PG, DD-PG or L-PG solution for 10 min. The glass slides were then rinsed with water several times to remove all excess and unbound polymer, and dried with a N_2 gun to obtain PG-, DD-PG- or L-PG-functionalized glass substrates. Scratches were made using a metallic doctor blade. Films thicknesses and roughness were analyzed (at least 20 different profiles for each sample) using the JPK SPM image processing software.

1.2.5 Contact angle measurements

For the contact angle measurements, substrates were incubated in a 0.1 mg mL^{-1} L-PG or PG water solution for 30 min at 21 °C, then rinsed with water to remove excess polymer. Excess water was removed by blowing the sample with a N_2 gun. Uncoated substrates were used as the control. Contact angle experiments were performed using H_2O (3 µL) at 21 °C on an optical contact angle tensiometer (DataPhysics) using the sessile drop method. The substrates were placed in the contact angle instrument window analysis. The drop shape was fitted using the elliptic method. The contact angle values and standard deviations were calculated based on the left and right contact angles of at least 15 different drops per sample.

1.2.6 Cytotoxicity assay

Cell viability was evaluated via a standard thiazolyl blue tetrazolium bromide (MTT) assay protocol. Cells (MDA-MB-231) were plated on a 96-well plate (Costar 3596, Corning, USA) with a seeding density of 10^4 cells per well in Dulbecco's modified Eagle medium (100 µL) with 10% fetal bovine serum. After 24 h, L-PG nanoparticles were added to the culture media (final concentrations as reported) and the systems were incubated for 24 h. Then, MTT reagent was added and after 4 h, the resulting formazan crystals were dissolved in DMSO. The cell viability was determined by absorbance measurements at 554 and 670 nm (as reference) with an Infinite M200 microplate reader (Tecan, Switzerland).

1.2.7 Degradation of PG and L-PG nanoparticles by β-amylase

The rate of glycogen particle hydrolysis by β-amylase was determined using the Somogyi–Nelson assay adjusted for a microtiter plate.[1] For the assay, a PG or L-PG solution (25 µL, 2 mg mL^{-1}) in 16 mM sodium acetate buffer (pH 4.8) was treated with β-amylase solution in H_2O (25 µL, 1 U mg^{-1}) for 20 min, 1 h, 2 h, or 24 h on a 96-well plate (Costar 3596, Corning, MA, USA); the experiments were performed in triplicates. After the incubation, the working solution was added (50 µL), the plate was covered and heated in a water bath at 95 °C for 20 min. Then, the plate was cooled to room temperature, and the arsenomolybdate color reagent was added (50 µL) into each well, followed by incubation for 1.5 h for complete color development. The absorbance was measured at 750 nm with an Infinite M200 microplate reader. To prepare the working solution, sodium potassium tartrate tetrahydrate (1.2 g), sodium carbonate (2.4 g), sodium bicarbonate (1.6 g), and sodium sulfate (14.4 g) were dissolved in water, and the resulting solution was diluted to 80 mL to obtain stock Solution I. Copper sulfate pentahydrate (0.4 g) and sodium sulfate (3.6 g) were dissolved in water, and the resulting solution was diluted to 20 mL to obtain stock Solution II. The solutions were stored separately to prevent copper oxidation.[2] Four parts of Solution I and one part of Solution II were freshly mixed to prepare the working solution before analysis. To prepare the color reagent, ammonium molybdate (2.5 g) was dissolved in water (45 mL) and concentrated sulfuric acid (2.1 mL). Sodium arsenate dibasic pentahydrate (0.3 g) was dissolved in water (2.5 mL) and mixed

with the ammonium molybdate solution. The reagent was incubated at 37 °C for 24–48 h and stored in a brown bottle.[3]

1.2.8 Stability of L-PG coatings on glass substrates

The chemical stability of the L-PG coatings was studied via fluorescence analysis. First, square-shaped glass slides were cleaned with ethanol (EtOH) and water and then completely immersed in a 0.1 mg mL^{-1} AF488-labeled L-PG solution for 10 min. Then, the functionalized glass substrates were rinsed with water several times to remove all excess and unbound polymer. The prepared glass substrates were then separately incubated for 60 min in several solutions: H_2O, 10 mM phosphate-buffered saline (PBS; pH 7.4), 1 M HCl, 1 M HNO_3, 1 M H_2O_2, 10 mM glutathione (GSH), 17 mM sodium dodecyl sulfate (SDS), EtOH, and 0.5 U mL^{-1} β-amylase (in 8 mM acetate buffer, pH 4.8). Following incubation, each glass slide was rinsed with water and dried with a N_2 gun. The fluorescence emission intensities were recorded by mounting the samples on a solid-state sample holder in a Fluorolog instrument (Jobin Yvon Horiba). Emissions intensities were recorded at a wavelength of 515 nm using an excitation wavelength of 488 nm (slit aperture 5). The data were recorded using the software FluorEssence.

1.2.9 Quartz crystal microbalance with dissipation (QCM-D)

QCM-D experiments were performed using a QSense E4 (Biolin Scientific, Sweden) equipped with a peristaltic pump. Before the measurements, gold sensor chips (QSX 301 Gold, Biolin Scientific) were cleaned with piranha solution, rinsed with Milli-Q water, dried with a N_2 gun and sterilized with a UV/ozone treatment (Bioforce Nanoscience, UV.TC.EU.003, USA) for 20 min.

1.2.10 Differential interference contrast (DIC) microscopy

DIC microscopy images were recorded using an inverted Olympus IX71 microscope.

1.2.11 Transmission electron microscopy (TEM)

For TEM analysis of the bare, L-PG- and L-PG/AuNP-coated PS microparticles, the corresponding water dispersion was dropped onto an ozone-cleaned copper grid and allowed to dry in air overnight. TEM images were acquired using a Tecnai Spirit (FEI, USA) instrument with an operation voltage of 120 kV.

1.2.12 Scanning electron microscopy (SEM) and energy-dispersive X-ray (EDX) spectroscopy

For SEM and EDX analysis, the sample-containing copper grid prepared for TEM analysis was attached onto a carbon tape and analyzed as is. SEM images and EDX spectra and mapping were acquired with a FlexSEM 1000 benchtop scanning electron microscope (Hitachi, Japan) equipped with a Quantax 80 EDX system (Bruker, USA). Typically, images and spectra of samples were recorded using a beam voltage of 15 kV, operating in SEM pressure mode and with an acquisition time of 5 min.

1.2.13 Scanning helium ion microscopy (HIM)

HIM was performed on an ORION NanoFab (Zeiss, Peabody, USA) using a 25 keV He^+ probe with a current of 0.3 pA, and the image was obtained using an Everhart–Thornley-type secondary electron detector. The sample was mounted on a 45° holder and the stage tilted by a further 30° to give a final viewing angle of 75°.

1.2.14 Stability of L-PG/AuNP hybrid coatings on glass substrates

To assess the chemical stability of the L-PG/AuNP hybrid coatings, square-shaped glass slides were first cleaned with EtOH and water and then completely immersed in a 0.1 mg mL^{-1} L-PG solution for 10 min. The functionalized glass substrates were then rinsed with water several times to remove all excess and unbound

polymer. The L-PG-coated substrates were then completely immersed in a AuNP colloidal suspension for 10 min and subsequently rinsed with water to obtain 1 bilayer coating of L-PG/AuNP on each side. The prepared glass slides were then separately incubated for 60 min in several solutions: H_2O, 10 mM PBS (pH 7.4), 1 M HCl, 1 M HNO_3, 10 mM $NaBH_4$, 1 M H_2O_2, *n*-hexane, EtOH, 17 mM SDS, and 10 mM GSH. After that, each glass slide was washed with water and dried with a N_2 gun. The UV–vis spectrum of each glass slide was recorded from 350 to 800 nm.

1.2.15 Catalytic evaluation of AuNPs in L-PG/AuNP-coated 15 mL polypropylene (PP) tubes

PP tubes functionalized with an inner coating of L-PG/AuNPs were used to perform the decoloration of methylene blue (MB; blue solution) to leucomethylene blue (LMB; colorless solution) via $NaBH_4$ in the presence of catalyst AuNPs. In a typical reaction, 5 mL of a 0.025 mM MB and 10 mM $NaBH_4$ solution were introduced into the tube and vortexed for 45 min. At intervals of 5 min, aliquots (0.3 mL) were withdrawn. The UV–vis spectra of the aliquots were measured using a plate reader in the range of 450 to 750 nm, with a recording interval of 2 nm. To obtain the kinetics graph, the absorbance intensity at 664 nm was recorded for each sample and plotted against the reaction time.

1.2.16 AuNP stability in modified 15 mL PP tubes

A 3-bilayer L-PG/AuNP-functionalized PP tube was prepared as described before, with AuNPs as the last layer. After each addition of AuNP solution, the supernatant was withdrawn and the UV–vis spectra were acquired. A 10 mM $NaBH_4$ solution (2 mL) was incubated by vortexing in the prepared tube for 45 min. At intervals of 5 min, aliquots (0.3 mL) were withdrawn. The aliquots were analyzed via UV–vis spectroscopy. To calculate the concentration (mM) of AuNPs in the supernatant, the following formula was used: OD@400nm:1.2 = 0.5 mM:*x* mM (where OD is the optical density).

1.2.17 Surface-enhanced Raman scattering (SERS) sensing using L-PG/AgNP hybrid coatings

A 3-bilayer L-PG/AgNP glass substrate was prepared as described before, with AgNPs as the last layer. Liquid samples at different concentrations of crystal violet were loaded onto the functionalized substrate and the SERS intensity was then measured with a RENISHAW Raman microscope equipped with a He−Ne laser operating at 532 nm. The laser spot size was 5 μm, focused by a 50× lens. Single scans were run with an integration time of 15 s using a grating of 1800 lines mm^{-1} from 300 to 1800 cm^{-1}. The acquired data were processed with the WIRE 2.0 software.

2 Figures

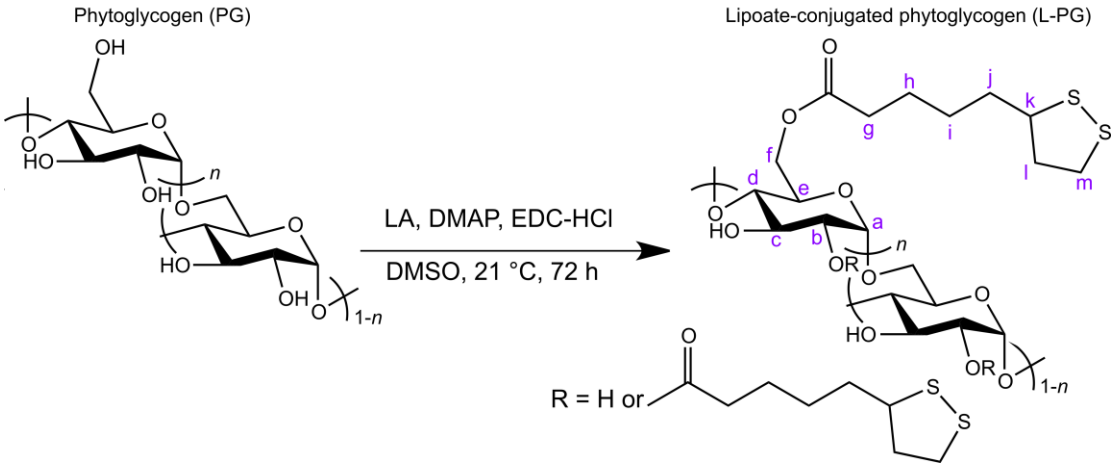

Figure S1: PG functionalization reaction with lipoic acid to obtain L-PG via Steglich esterification.

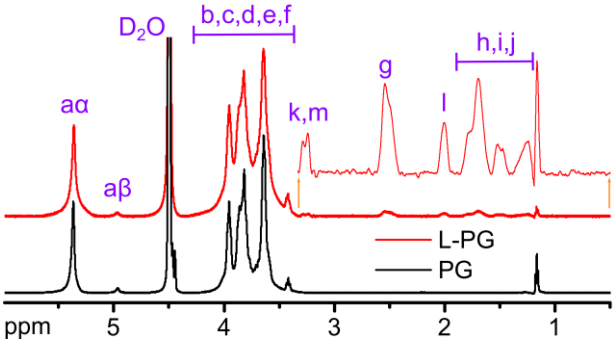

Figure S2: H-NMR spectra of L-PG and PG. The thin red line is a magnification of the lipoate peaks from 3.4 to 0.5 ppm.

Table S1: Chemical modification reactions of PG into L-PG

Type of glycogen	Targeted degree of functionalization (LA/glucose mol/mol)	Actual degree of functionalization (LA/glucose mol/mol)	Solubility
PG	30	Not measured	Non-soluble in water, EtOH, DMSO, or *n*-hexane
PG	20	Not measured	Non-soluble in water, EtOH/water (50:50), or DMSO
PG	10	2% on total glucose, 10.6% on H4 terminal	Water soluble, up to 20 mg mL^{-1}
PG	3	Below H-NMR limit of detection	Water
PG	1	Below H-NMR limit of detection	Water

PG, phytoglycogen; EtOH, ethanol; DMSO, dimethyl sulfoxide.

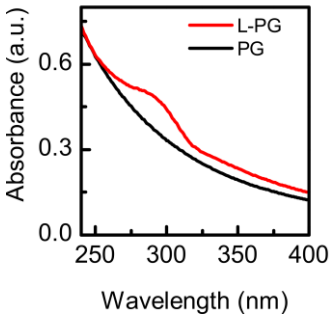

Figure S3: UV–vis spectra of L-PG and PG.

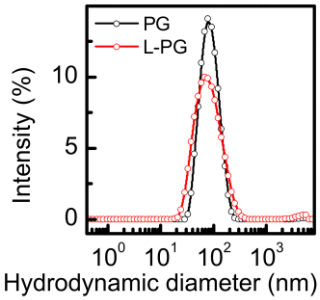

Figure S4: DLS hydrodynamic diameter populations of L-PG and PG.

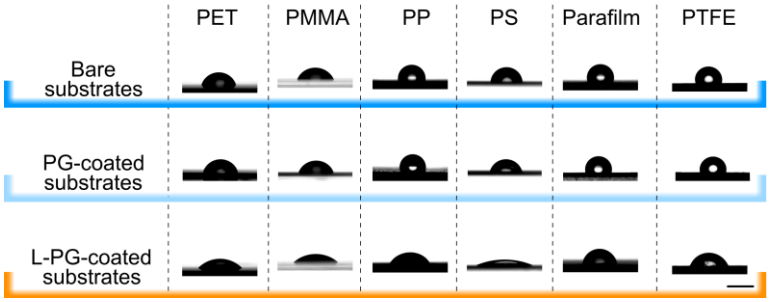

Figure S5: Photographs of water droplets on bare, PG-, and L-PG-coated substrates; the contact angle values are given in Figure 2c. Scale bar: 2 µm.

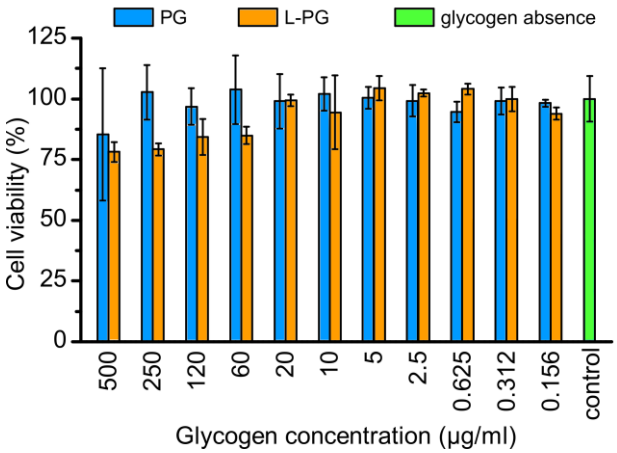

Figure S6: Cytotoxicity studies of PG and L-PG.

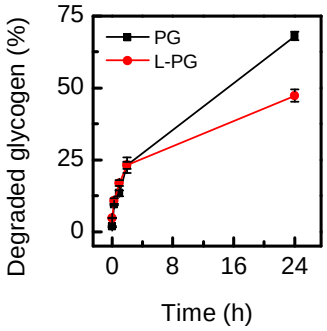

Figure S7: Enzymatic degradation of PG and L-PG.

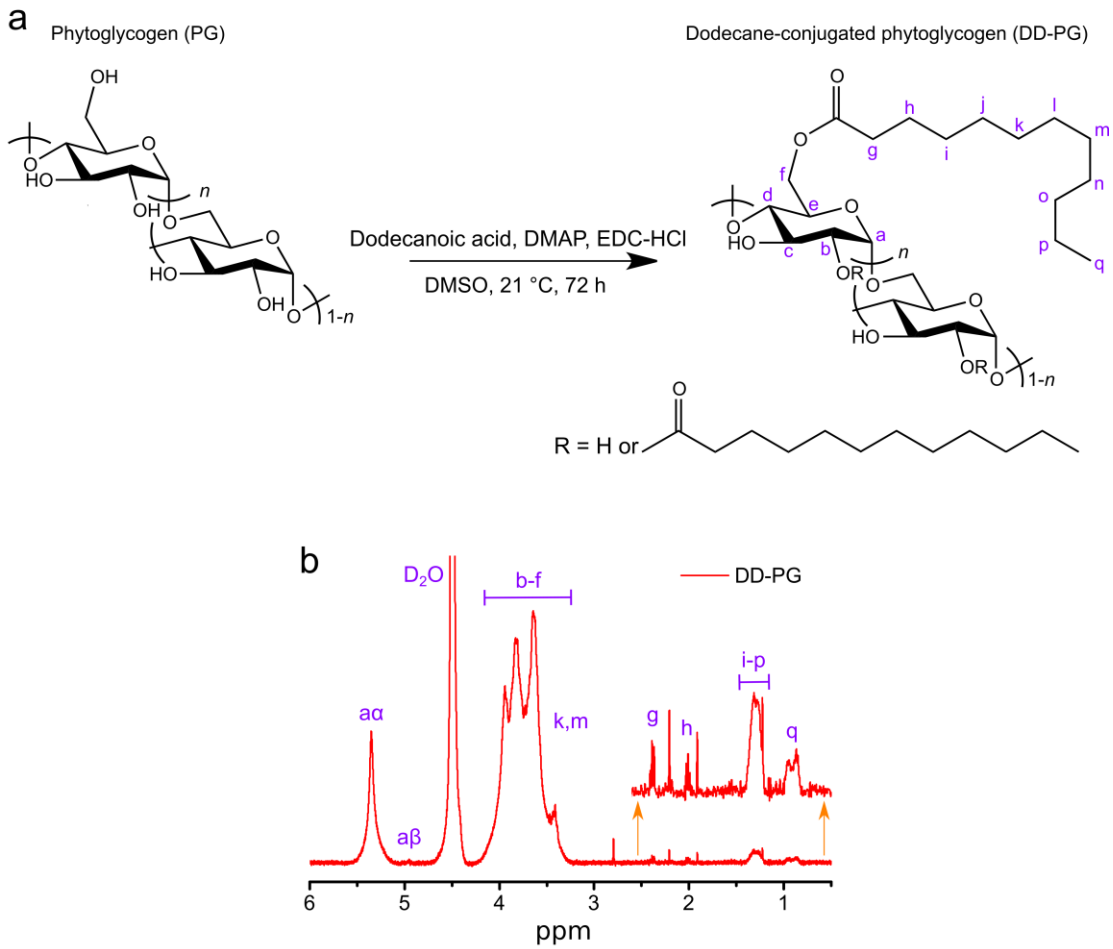

Figure S8: (a) PG functionalization reaction with dodecanoic acid to obtain DD-PG via Steglich esterification and (b) H-NMR spectra of DD-PG with magnification of the peaks corresponding to the dodecane moiety from 2.5 to 0.5 ppm.

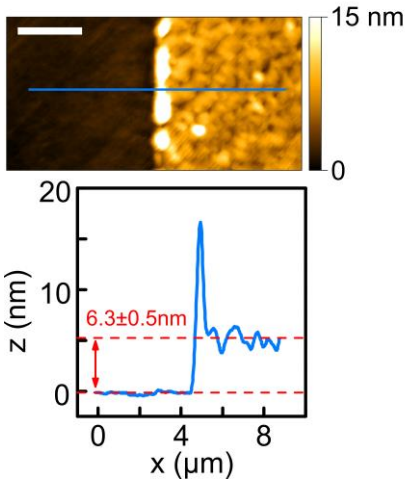

Figure S9: Dry-state AFM image and corresponding height profile of DD-PG-coated glass substrates (scale bar = 2 μm).

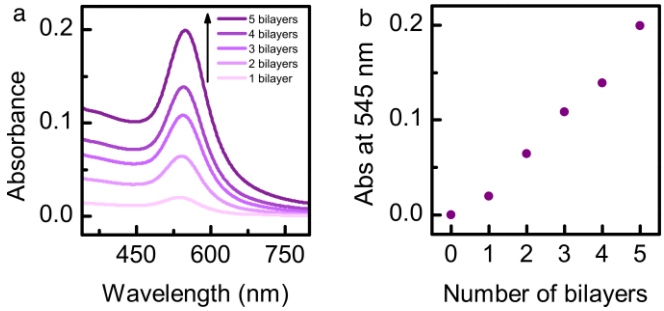

Figure S10: (a) UV–Vis spectra of glass substrates coated with increasing number of L-PG/AuNP bilayers. (b) Localized surface plasmon resonance absorbance profile at 545 nm as a function of the bilayer number.

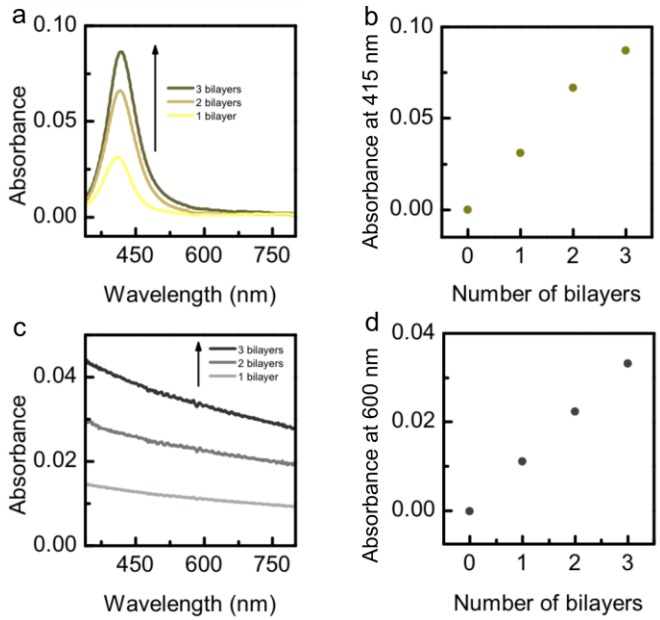

Figure S11: UV–Vis spectra of glasses coated with increasing number of (a) L-PG/AgNP and (c) L-PG/PtNP bilayers with corresponding absorbances at (b) 415 nm and (d) 600 nm as a function of the bilayer number.

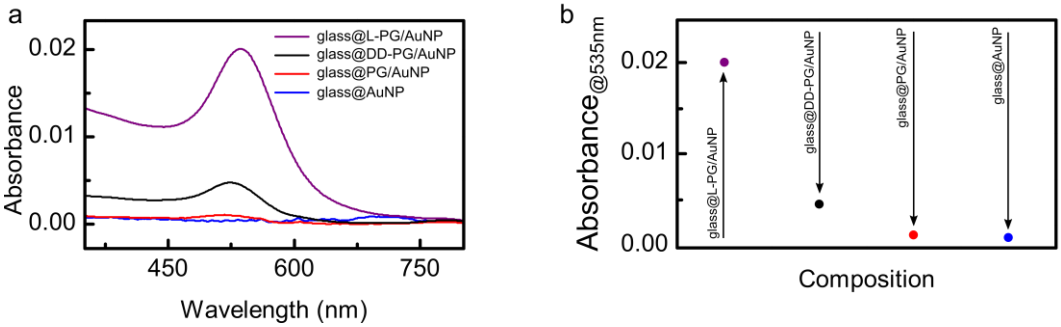

Figure S12: (a) UV–Vis spectra of glass substrates coated with L-PG/AuNP, DD-PG/AuNP, PG/AuNP assemblies or AuNPs alone and (b) corresponding absorbances at 545 nm.

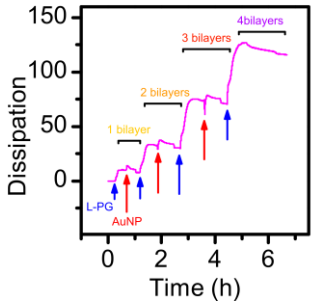

Figure S13: QCM-D dissipation profile of an L-PG/AuNP LbL assembly on gold chip obtained upon sequential deposition of L-PG (blue arrow) and AuNPs (red arrow); the corresponding QCM-D frequency profile is shown in Figure 3b.

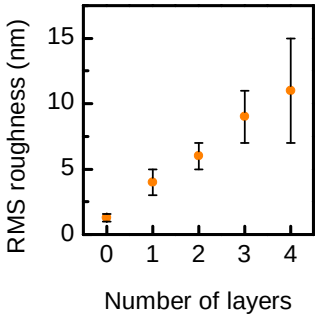

Figure S14: Root mean square (RMS) roughness of dry films as a function of the L-PG/AuNP bilayer number.

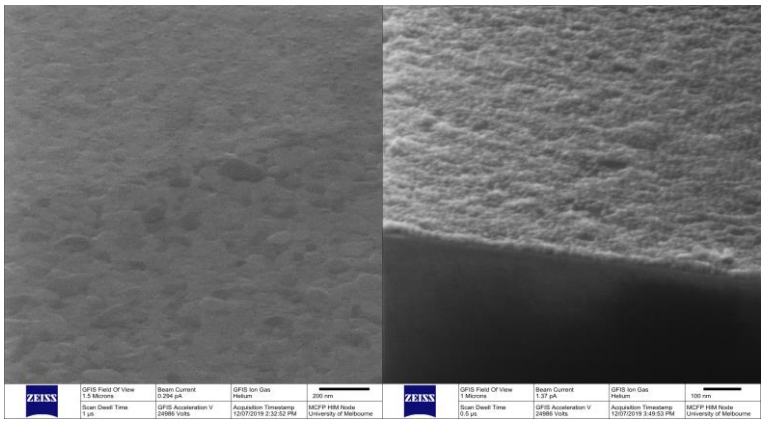

Figure S15: HIM images of L-PG/AuNP LbL assembly on glass with the final layer as L-PG (left) and AuNP (right).

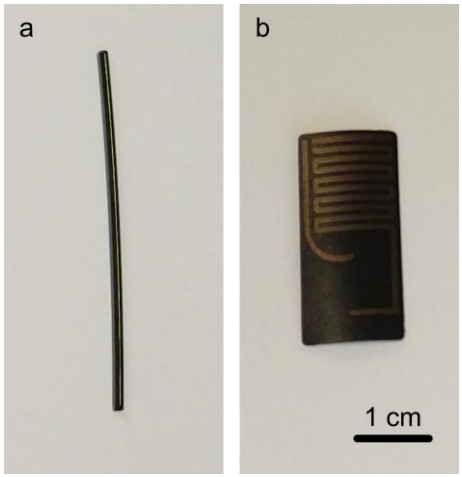

Figure S16: Photographs of L-PG/AuNP assembly on (a) polyether ether ketone and (b) Viton.

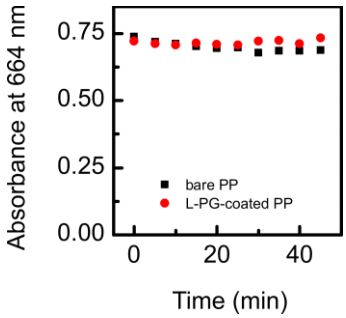

Figure S17: Degradation kinetics of MB via $NaBH_4$ on a bare PP tube and L-PG-coated PP tube. Both reaction systems do not contain AuNPs.

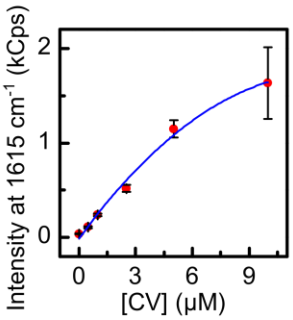

Figure S18: SERS signal intensity at 1615 cm^{-1} as a function of the concentration of the crystal violet (CV) solution; the corresponding SERS intensity profiles are shown in Figure 5d.

3 References

(1) Y. Shao and A. H.-M. Lin, *Food Chem.,* 2018, **240**, 898.
(2) M. Somogyi, *J. Biol. Chem.,* 1952, **195**, 19.
(3) N. Nelson, *J. biol. Chem.,* 1944, **153**, 375.